Mitigating Effects of Interference in On-Chip Antenna Measurements

Edmund C. Lee, Edward Szpindor
ORBIT/FR, Inc.
Horsham, PA, USA
edmund.lee@orbitfr.com

William E. McKinzie III
WEMTEC, Inc.
Fulton, MD, USA
will@wemtecinc.com

Abstract—Coupling a Chip Antenna to an Antenna Measurement System is typically achieved using a coplanar micro-probe. This micro-probe is attached to a probe positioner that is used to maneuver the micro-probe into position and land it on the chip. Through this process, the chip antenna is supported by a dielectric chuck. Intentional and unintentional radiation from the chip antenna will interact with the micro-probe and dielectric chuck. From design conception, the antenna designer must take steps to reduce ground plane currents on the chip antenna surface to minimize unintended radiation that will interact with both the measurement setup and the surrounding components of the final in-situ design. Even with good design practices, residual ground plane currents will still remain and radiate from the chip antenna. Combined with intentional radiation from the chip antenna in the upper hemisphere, these radiated fields will illuminate the micro-probe and the probe positioner. Scattered fields from both the micro-probe and its positioner will superimpose with the antenna's direct radiated fields to generate interference patterns with the desired signal at the spherical measurement probe. In this paper, we evaluate, on a first order, these effects by experimentation on two brands of micro-probes (ACP & Infinity). The residual errors are then evaluated using modal filtering that further reduces these effects and the results are presented. Finally the dielectric chuck is modeled in simulation to evaluate the impact of the chuck on antenna patterns at 60 GHz and the results are presented.

I. INTRODUCTION

On-chip antennas at millimeter wave frequencies are being developed and deployed into useable applications, such as in the growing WiGig standard alliance, to achieve gigabit data rates. Researchers have investigated both antenna characterization and low cost, highly integrated packaging based on the potential of silicon technologies, particularly at 60 GHz [1]. Therefore, the need for a probe-based measurement setup with proper design and understanding is needed to be able to minimize the errors and to attain accuracy in measurements.

Several key features of the probe-based measurement setup include use of a micro-probe, a micro-probe positioner, and a chuck holder for the on-chip antenna—all of which can cause unintentional radiation. However, proper mitigation of the unintentional radiation should not be limited only to the measurement setup itself. From design conception of the on-chip antenna, the antenna designer must also take steps to reduce currents on the chip substrate, which will interact both with the measurement setup itself as well as the surrounding components of the final design and package. Even with good design practices in the antenna design and measurement system, residual currents and reflections will still remain and generate interfering patterns with the desired AUT measurements. This paper will evaluate these effects in the 60 GHz frequency band.

II. MEASUREMENT SETUP & ANTENNA DESIGN

The measurement accuracies for probe-based on-chip measurements at millimeter waves is determined both from a good antenna design and measurement environment.

A. Antenna Design

The antenna design is paramount to being able to evaluate an antenna properly in a probe-based measurement environment. Due to the physical location of the micro-probe and its positioner, there will always be a solid angle associated with radiation blockage, potential multipath interference, and crosstalk on the underside of the probe where the measurement system will not be able to measure as accurately. Typically, radiation blockage is in the upper hemisphere and in the plane of the micro-probe. An antenna designed for experiment, specifically for a probe-based measurement system, will allow for proper characterization of the antenna itself. For a planar on-chip antenna, the designer can design the feeding structure such that the probe landing pads feed into the antenna at orthogonal planes to the radiating element(s). For example, on a patch, the probe landing pads can be lined up with the E-plane in one configuration and with the H-plane in a second configuration. This will allow for minimum RF interference effects from the probe in one principal plane while also being able to fully measure the orthogonal principal plane. By measuring the second configuration, the other principal plane would also be able to be measured more fully with minimum interference effects. Additionally, the designer could choose to radiate either as an endfire antenna (away from the probe), into the lower broadside direction, or into the upper broadside direction. The main beam direction will depend on the type of application the antenna will be used for and its desired directivity.

Induced surface waves can be another major source of errors in on-chip antennas, especially at millimeter waves due to electrically thicker substrates [2]. In broadside-radiating antennas in substrates such as low temperature co-fired ceramic

(LTCC) that have medium relative permittivity (4< εr<10), transverse magnetic (TM) mode surface waves are a known issue and will diffract at edges of ground planes and cause pattern distortion [2]. Electromagnetic bandgap (EBG) structures such as the Sievenpiper EBG structure can be used for wave suppression as in [2], which also has a small enough profile to fit into on-chip scale packages for millimeter wave. This methodology has successfully been demonstrated in [2] to suppress the surface waves and thereby increase broadside directivity by approximately 5 dB, which shows the potentially large impact unwanted surface waves can have on expected antenna performance and measurements.

B. Measurement Setup

The measurement was performed in an Orbit/FR µLab as seen in Figure 1(a), which is a spherical coordinate measurement chamber with a stationary probe station capability. This measurement setup consists of several key components that can impact measurement accuracy. The coplanar probe is typically the method of choice for launching RF energy into the on-chip antenna. This paper will only discuss ground-signal-ground (GSG) probes which are typically the most often used due to its advantage in tightly controlling the fields around the signal probe [3]. The probe and dielectric chuck holder are positioned along the X-axis in the spherical coordinate system as shown in Figures 1(b) and 2.

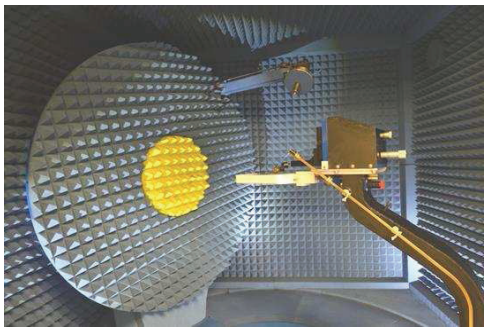

Figure 2(a): Orbit/FR µLab on-chip measurement setup

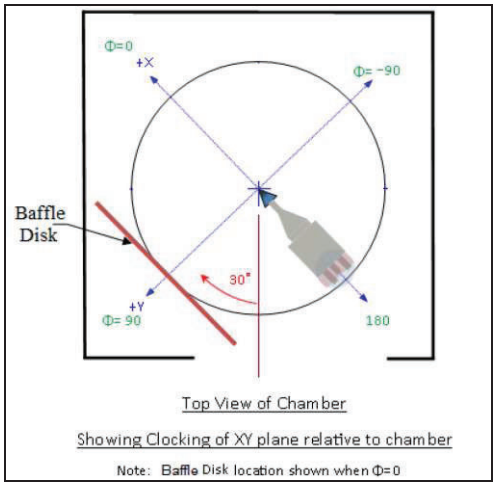

Figure 3(b): µLab Coordinate System (top view)

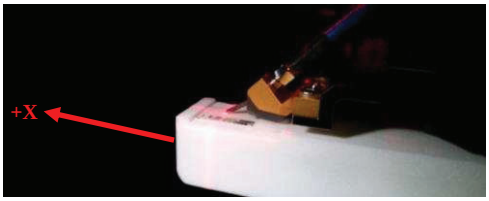

Figure 1(a): Chuck holder with ISS mounted and landed air coplanar probe (ACP)

The AUT consists of the 60 GHz patch antenna as described in [2] with integrated Sievenpiper EBG structures. A Cascade impedance substrate standard (ISS) was used for the terminated load at the tips of the probe. The radiated pattern of the termination is measured and subtracted from the AUT pattern, which will be discussed more in depth later as a way to separate probe radiation from the AUT radiation. Figure 2a shows the measured load micro-probe location on the ISS, which is located approximately 19 mm (0.75 inches) from the center of the measurement sphere. This is also the same landing location for the on-chip AUT.

Two different frequently-used families of probes from Cascade MicroTech were evaluated to see their effects on the measured patterns—ACP and Infinity. A 150 um pitch was used for both probes. Typically ACP probes have better visibility at the probe tips to allow for more accurate probe-landing placement, whereas the Infinity probe has more highly-confined fields to reduce unwanted coupling.

III. Measurement Results

The on-chip LTCC patch with EBG structures was measured and is named 60c (Figure 2b). The first set of measurements will show the matching accuracy between the two probes. The second set of measurements will show the probe effects on the radiated patterns as well the results of subtracting these unwanted probe-based scattered fields to produce a more accurate representation of the true AUT patterns. The last set of results will show the impacts of modal filtering on measured data and how that alternate methodology can produce quite accurate patterns that are similar to the probe subtraction-based methodology.

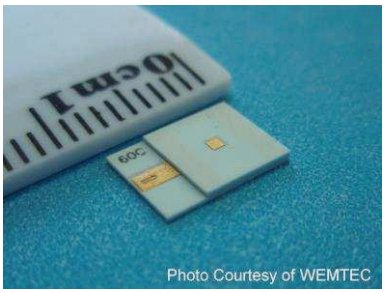

Figure 2(b): 60c LTCC patch antenna with integrated EBG structures

A. S11 Impedance Matching

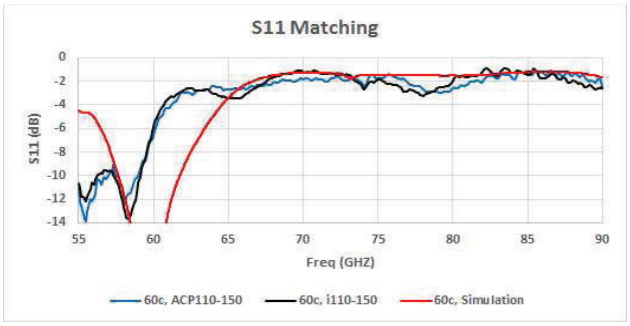

Figure 3: Impedance Match for ACP (blue), Infinity (black), and simulation (red) on AUT (60c)

The accuracy of the impedance matching does differ between the two probes as shown in Figure 3. Resonance occurs at 58 GHZ on the AUT for both probes and matches fairly well with simulation. The matching is approximately -12 dB for the ACP and -14 dB for the Infinity, which appear slightly detuned, possibly due to tolerance accuracies of the traces and patch in the AUT. The different S11 behavior between the two probe families may be due to parasitic differences as seen from the radiation resistance in the probes, which can cause different accuracies in the initial 1-port calibration. Therefore, different serial numbered probes of the same family will exhibit minimal S11 differences when landing, which has been verified in measurements with the Infinity probe.

B. Principal Plane Patterns (60c) Using Load Subtraction

A measurement with the probe terminated on an ISS load was used to perform a subtraction on the AUT measurements (which have probe radiation errors superimposed into its patterns). The intent of this methodology is to separate the effects of the probe radiation from the AUT radiation. The 60c (AUT) has a return loss of approximately 14 dB (96% power transfer) at 58 GHZ, while our ISS termination load has a measured return loss of approximately 30 dB (99.9% power transfer) across the frequency band. The assumption is that the ~3.9% power transfer difference is minimal enough to be able to perform pattern subtraction at resonance. The impedance match on both the 60c and termination load is very good.

Looking at Figures 4 and 5, the ACP probe was used to land on the ISS load. As shown in dark red, there is a significant radiation pattern that reaches levels as high as -15 dBi in the principal planes despite a having a good impedance match. This radiation can come from several sources, which may include interaction with other metal on the ISS itself as well as the body of the probe.

Performing a subtraction of the load and 60c radiation patterns (orange line), we see that the E-plane (XZ-plane) does not exhibit much effect from the probe radiation, especially around the main beam due to the large dB separation (20+ dB) between the 60c and load at those particular angles. Some effect occurs near $\theta = \pm 180^{o}$, where the 60c side lobes are much lower (within ~8 dB). Note that the gain dropout between $\theta = -130^{o}$ and -50^{o} is due to physical probe station blockage. The H-plane (YZ-plane) exhibits more significant impacts, both around $\theta = \pm 30^{o}$ and $\pm 60^{o}$.

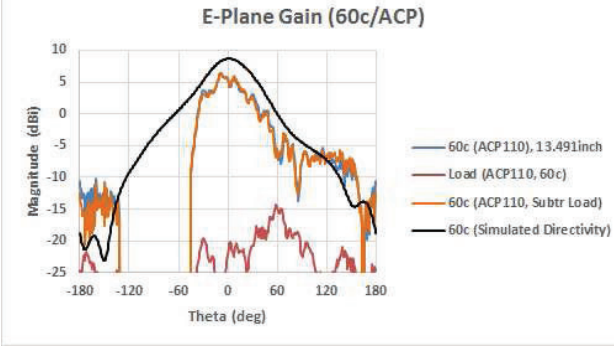

Figure 4: E-plane (XZ-plane) gain measurement on 60c using the ACP probe.

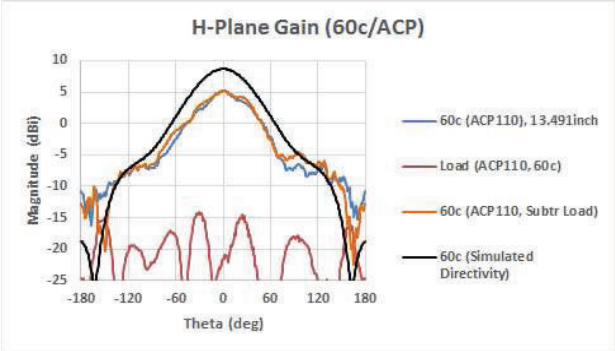

Figure 5: H-plane (YZ-plane) gain measurement on 60c using the ACP probe.

Table I shows the expected max signal level error for a measurement based on the interfering signal level below the peak. If we look at the H-Plane plot in Figure 5 near $\theta = \pm 110^{o}$, we see the load radiation (red) is approximately 13 dB below our 60c signal level (orange). The delta between the un-subtracted pattern and subtracted pattern is approximately 0.6 dB. According to Equation (1), this correction falls within the expected maximum amplitude errors with its differences in levels due to several factors including (1) different return losses between the AUT and load and (2) slight misalignments and spatial location differences during physical insertion of the ISS load and AUT into the system. Small phase variances from subtraction and addition throughout the system will also lead to amplitude variation errors.

$$\text{Signal Error} = 20 * \log(1 \pm e^{[SNR/20]}) \qquad (1)$$

TABLE I. SIGNAL ERROR LEVEL (EQUATION 1).

Interfering Signal Level Below Peak (dB)	Maximum Amplitude Error (dB)	
	Plus	Minus
-10	+2.387	-3.302
-20	+0.828	-0.915
-30	+0.270	-0.279
-40	+0.086	-0.087
-50	+0.027	-0.028

Looking at Figures 6 and 7, the Infinity probe was used on both the ISS and 60c. As seen in the E-plane, the peak load levels are fairly low at -20 dBi in the main lobe of the 60c. For this reason, we do not see significant error on our 60c measurements. In the H-plane, we also have fairly low peak load levels of -17 dBi, but there is a significantly wide pattern spanning from θ = +50º to +150º, which shows in our corrected 60c pattern (red). Note that the dropout between θ = -130º and -50º is due to physical probe station blockage.

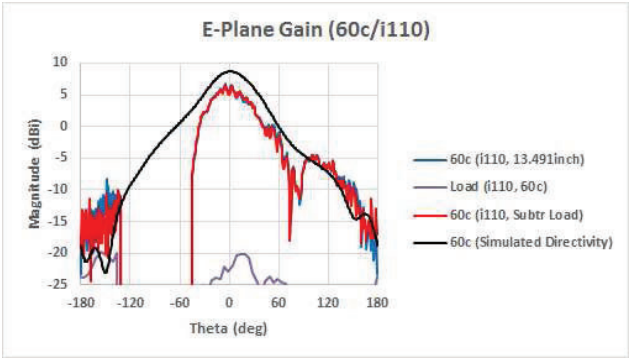

Figure 6: E-plane (XZ-plane) gain measurement on 60c using the Infinity probe.

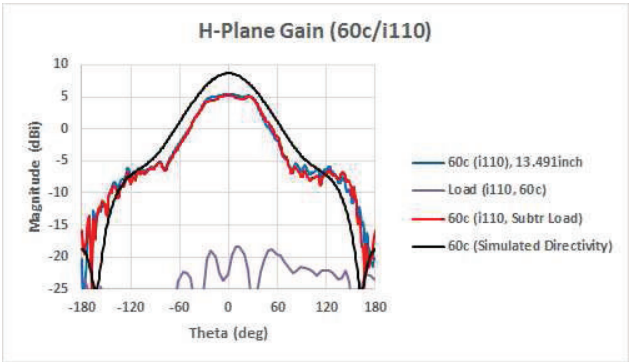

Figure 7: H-plane (YZ-plane) gain measurement on 60c using the Infinity probe.

The principal plane cuts shown in Figures 4-7 show a peak simulated directivity of approximately 8 dBi and with a simulated efficiency of approximately 83%. Our measured data has slightly lower efficiency, and the difference is likely due to internal 60c antenna structures that could benefit from more accurate fabrication and are lossier than expected. It also appears that the Infinity probe has less radiation compared to the ACP probe by approximately 5 dB or more. Therefore, the best accuracy will be obtained using the Infinity probe.

Taking a closer look at the ACP and Infinity measurements, we can see that in the H-Plane, correction on the ACP pattern produces a flatter pattern at boresight. We see that with the ACP probe, antennas radiating in the upper broadside hemisphere will be perturbed by the probe itself. However, the Infinity probe will not perturb the upper hemisphere as much. This same flatter phenomenon is seen in the Infinity probe even without correction, and we have already seen that the Infinity probe does in fact already exhibit a more accurate pattern in terms of how much impact the probe radiation has on the AUT measured pattern.

C. Principal Plane Patterns (60c) Using Modal Filtering

Another type of correction that can be used to separate the probe radiation effects from AUT is spherical modal filtering, which we will see is comparable to the load subtraction correction that was implemented above. This technique is demonstrated in [4] and is a spatial-filtering technique that takes advantage of the fact that scattering interferers vary more rapidly than λ on the AUT's minimum enclosing spherical surface [4]. The high oscillating interferers, then, are attributed to higher-order modes which can be filtered in the spherical modes domain in order to isolate the radiating sources, which we want to limit to the antenna itself. As discussed in [4], then, the minimum number of modes required to fully represent the antenna depends on the physical electrical size of the AUT. We will focus solely on the ACP probe in this section to demonstrate the technique on the higher radiating probe since its filtering effects will be more easily seen.

The maximum radiating modes (N_{Max}) for an antenna with minimum sphere of diameter D_{Min} is described by:

$$N_{Max} \approx \pi (D_{Min}) / \lambda, \quad (2)$$

The minimum Nyquist sampling increments on the measured sphere is described by:

$$\theta_{Min\ Sample}, \phi_{Min\ Sample}\ (\text{radians}) = \lambda / D_{Min}, \quad (3)$$

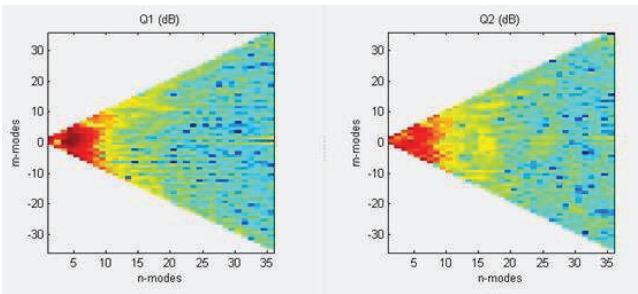

Figure 8: Full spherical modal expansion shows radiation is concentrated in the lower modes for the 60c antenna.

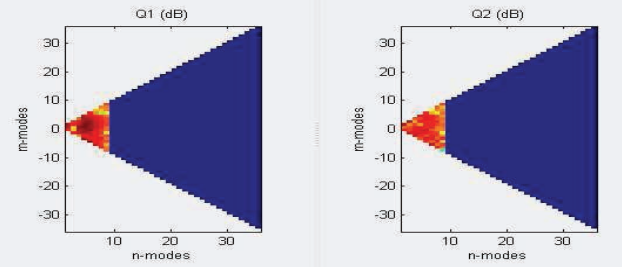

Figure 9: Modal filtering captures only the 60c antenna as a radiation source and filters out extraneous scattering sources.

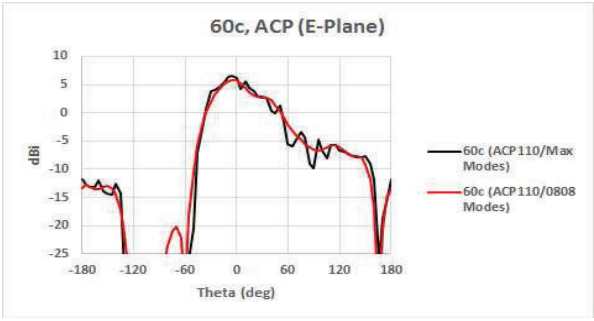

Figure 10: E-plane (XZ-plane) gain measurement on 60c using the ACP probe with modal filtering.

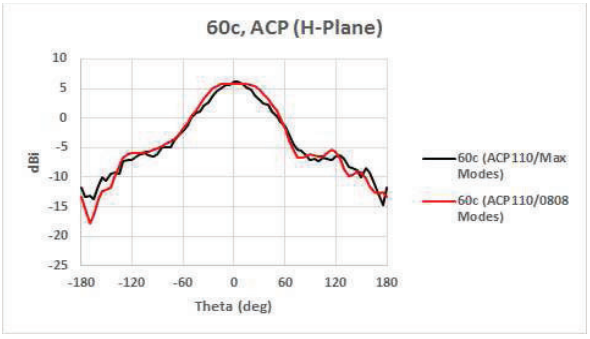

Figure 11: H-plane (YZ-plane) gain measurement on 60c using the ACP probe with modal filtering.

The 60c antenna consists of a patch and EBG structures that form an 8.25 mm (0.325 inch) diameter minimum sphere. This excludes the probe transition that feeds the patch. According to Equation (2), based on this electrical length of the 60c in the 60 GHz band of interest, the maximum number of physical modes that can be excited is 5. However, due to a 4mm offset in the +Z direction based on the location of the chip antenna while sitting on the chuck, the minimum enclosing sphere increases to a 12.33 mm (0.4825 inches) diameter. This translates to approximately 8 maximum modes that can be excited for the AUT. Additionally, according to Equation (3), the minimum Nyquist sampling increment on this sphere is 24 degrees. This measurement has been sampled at 5 degree increments, which allows for a high-resolution, detailed measurement that is more than sufficient to capture all the radiating energy. Figure 8 shows that most of the energy is found in the lower modes for such a small antenna. Filtering down to 8 modes using MV-Echo (Figure 9) allows for a more accurate representation of the true radiating sources which are focused on the AUT patch and EBG structures.

Figures 10 and 11 show the effects of modal filtering in red. It is seen that the lowest 8 TM and TE modes are responsible for radiation in this patch. Note that this filtering was performed with a 5º sampling increment instead of 1º to decrease measurement time to an acceptable time and since Nyquist is satisfied. Thus, the patterns will be expected to look slightly smoother than is seen in previous measurements in this paper. Several features show up that are common to the results of the load subtraction correction performed above. There again is minimal correction impact in the E-plane. In the H-plane, we see a flattened pattern near boresight similar to the load subtraction correction. The advantage of this modal filtering is that there is no need to measure the effects of the micro-probe landed on the load. Additionally, this filters out any other radiating sources that may include effects such as the dielectric chuck, probe, and probe-transition.

D. Effects from Dielectric Chuck AUT Holder

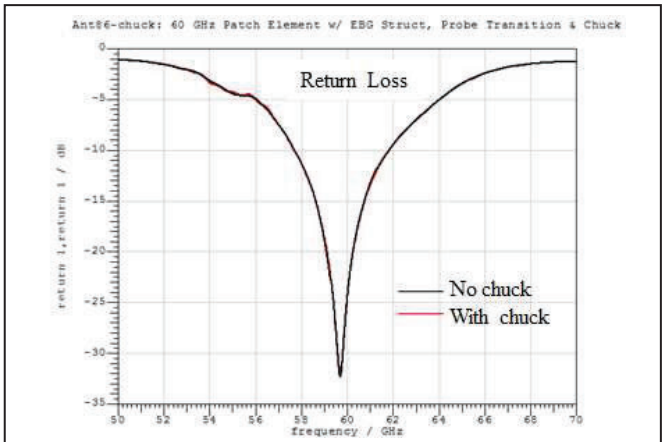

Figure 12: Return loss effects are minimal with the dielectric chuck

The dielectric chuck used to hold the AUT is a low permittivity Rohacell HF51 Styrofoam. The εr is 1.05 with an estimated loss tangent of 0.04 at 60 GHz. The loss tangent was estimated, but no data at 60 GHZ is available to the author's best knowledge. Currently, there are plans to measure these material properties using a waveguide resonant cavity. The chuck is approximately 1"x1"x4" in size with the AUT sitting on top and its main beam radiating above the chuck.

A simulation was run using the 60c antenna supported by the chuck and suspended in free space. As seen in Figure 12, there is essentially no impact on the return loss due to the chuck. There is minimal impact on the realized gain, as seen in Figure 13, of approximately 0.2 dB due to the chuck. Figure 14 shows the E-plane directivity with a ripple between θ = +90º and +120º, which is also seen in the measurements in previous sections. This indicates the presence of traveling waves that are guided by the dielectric chuck and most noticeable along the negative X-axis where the chuck has the longest reach beyond the antenna. Interestingly enough, the modal filtering

does correct and filter out this ripple in the E-plane as well. The H-plane is slightly impacted at the shoulders with the chuck, as is seen in Figure 15.

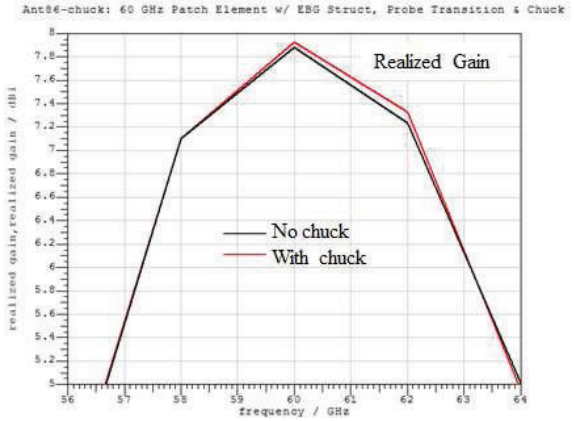

Figure 13: Realized gain effects are minimal with the dielectric chuck.

Figure 14: E-plane (XZ-plane) impact of chuck

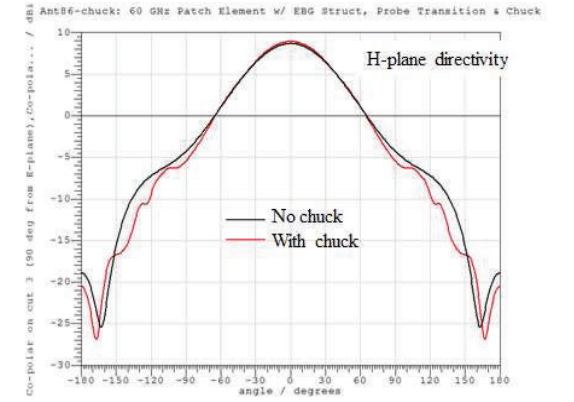

Figure 15: H-plane (YZ-plane) impact of chuck

IV. CONCLUSIONS

Measurements for the 60c anteenna and other on-chip millimeter wave antennas have many challenges that can be impacted by multiple factors in the measurement system, one of which is the probe itself. Two methods for analysis and correction of these factors have been presented—load pattern subtraction and modal filtering. The load pattern subtraction was successfully able to correct for the impacts of the probe radiation, and this was seen using a comparison of ACP and Infinity probes. The Infinity probe was found to radiate much less and have more accurate measurements for our antenna compared to the ACP probe. However, the infinity probe does not solve the issues stemming from the dielectric chuck and traveling waves on the chip substrate itself. The load pattern subtraction will not correct for the traveling waves either. The spherical modal filtering appears to be the most accurate of the two methodologies in eliminating the impacts of other radiating sources, such as the dielectric chuck. It also allows for a quicker measurement time since only one measurement will need be made.

When making measurements, the majority of unwanted radiating sources can be corrected during post-processing. However, the challenges of millimeter wave necessitates the need for very fine precision and accuracy of the measurement system and on-chip antenna features, which have been accomplished thus far. Those tolerances are typically orders of magnitudes more accurate compared to the error magnitudes for placement of the chip. Very accurate knowledge of the placement of the AUT inside the measurement sphere is critical, as it can create errors in the type of post-processing assumptions and analysis. However, the modal filtering technique can be processed in such a way as to be more conservative and to allow a larger number of modes to be passed thru the filter. In this manner, spherical modal filtering is a very powerful tool that allows for flexibility in post-processing to allow for the most accurate measurement correction.

REFERENCES

[1] A. Bisognin, D. Titz, F. Ferrero, G. Jacquemod, R. Pilard, F. Gianesello, D. Gloria, C. Laporte, H. Ezzeddine, D. Lugara, C. Luxey, "Probe-fed measurement system for F-band antennas," Antennas and Propagation (EuCAP), 2014 8th European Conference, pp. 722-726, 2014.

[2] W. E. McKinzie III, D. M. Nair, B. A. Thrasher, M. A. Smith, E. D. Hughes, and J. M. Parisi, "60 GHz patch antenna in LTCC with an integrated EBG structure for antenna pattern improvements," Antennas and Propagation Society International Symposium (APSRSI), July 7-12, 2014, pp. 1766-1767.

[3] Scott A. Wartenberg. RF Measurements of Die and Packages. Boston: Artech House, 2002. Print.

[4] L.J. Foged, L. Scialacqua, F. Mioc, F. Saccardi, P.O. Iverson, L. Shmidov, R. Braun, J.L. Araque Quijano, and G. Vecchi, "Echo suppression by spatial-filtering techniques in advanced planar and spherical near-field antenna measurements," IEEE Antennas and Propagation Magazine, Vol. 55, No. 5, pp. 235-242, Oct 2013.